Appl. Phys. B 69, 217–222 (1999) / Digital Object Identifier (DOI) 10.1007/s003409900074

Applied Physics B
Lasers
and Optics

Efficient magnetic guiding and deflection of atomic beams with moderate velocities

A. Goepfert, F. Lison, R. Schütze, R. Wynands, D. Haubrich, D. Meschede

Institut für Angewandte Physik, Rheinische Friedrich-Wilhelms-Universität Bonn, Wegelerstr. 8, D-53115 Bonn, Germany
(Fax: +49-228/733-474, E-mail: sek@iap.uni-bonn.de)

Received: 9 November 1998/Revised version: 6 April 1999/Published online: 30 July 1999

Abstract. We have studied guidance and deflection of a beam of cesium atoms by a strong toroidal magnetic quadrupole field. The beam guide is made from permanent magnets sustaining a radial field gradient of 2.8 T/cm. Atoms with moderate longitudinal velocities ranging from 30 m/s to 70 m/s were inserted across the 10-mm-diameter aperture of a 24.5° arc with radius 300 mm. We have measured transmission and beam divergence and find good agreement with ray-tracing calculations and analytical estimates. The magnetic beam guide allows for 100% transmission of heavy atoms over large angles.

PACS: 03.75Be; 32.80Pj; 07.55.w

The availability of slow and intense atomic beam sources prepared by laser cooling techniques has given rise to the development of many atom optical components for the precise manipulation of atomic trajectories [1]. Besides atomic mirrors, lenses, beamsplitters, and diffraction gratings atomic waveguides have gained increasing interest during the past years. Several different schemes have been proposed for transverse confinement using the interaction of atoms with inhomogeneous magnetic [2–4], electric [5], or light fields [6]. Atomic guides find a variety of applications. They are, for example, used to transfer atoms from a preparation stage to the experimental region [7–10], in close analogy to the transport of light by optical multimode fibers. Guiding atoms in specially tailored light fields ($\mathrm{TEM}^{*}_{0,n}$ "doughnut" modes) and applying additional cooling methods allows one to increase the phase-space density of atomic beams [11]. A challenging extension of these schemes, which would resemble the optical single-mode fiber, is to cool atoms down to the lowest transverse vibrational state in an atomic waveguide with very steep transverse gradients to achieve one-dimensional systems of atomic gases [12].

Most of the guiding experiments so far performed make use of the optical dipole force in a near resonant inhomogeneous light field. Systems based on magnetic dipole forces offer an interesting alternative, because they can be applied to all atoms and molecules with nonzero magnetic moment. Permanent magnetic materials with high remanence force are readily available and can be used for the construction of guiding devices with high magnetic gradients, high potential energies at the boundaries, and large apertures. Once built, these devices are very reliable, compact, and essentially maintenance-free. It is straightforward to expand a toroidal magnet system at relatively large radii of curvature to any desired length of arc. Even a full 360° superconducting hexapole ring has been constructed as a storage device for cold neutrons for the determination of the neutron mass [13].

The treatment of atomic motion in an inhomogeneous magnetic field is very much simplified if the magnetic moment $\boldsymbol{\mu}$ adiabatically follows the magnetic field lines. This is the case for atoms with moderate velocities moving in slowly varying magnetic fields and also applies to our situation. Then paramagnetic atoms experience a force that can be expressed by the spatially varying scalar amplitude of the magnetic flux density B as $\boldsymbol{F}_{\mathrm{mag}} = -\mu_{\mathrm{eff}} \nabla B$, where $\mu_{\mathrm{eff}} = \partial E/\partial B$. For most applications it is preferable or even essential to prepare the atoms in a magnetic substate with a maximum component of the magnetic moment antiparallel to the external magnetic field ($m_J = +J$). These "low-field seekers" usually have an effective magnetic moment of one or two Bohr magnetons μ_{B} which is independent of the local magnetic field strength.

Transverse confinement of paramagnetic atoms in low-field seeking states is obtained by all multipole configurations with an axial field minimum. We have chosen the quadrupole configuration for our experiments, which is simple to construct mechanically, at the same time yielding higher field strengths at the aperture [14] and tighter confinement to the axis than higher order multipole field configurations. The force acting in the radial direction is independent of the distance $\rho = (x^2 + y^2)^{1/2}$ from the axis and for a curved arrangement the minimum radius of deflection hence is given by

$$R = \frac{mv^2}{\beta}\,, \tag{1}$$

where $\beta = \mu_{\mathrm{eff}}\,\mathrm{d}B/\mathrm{d}\rho$. We have collected the maximum velocity compatible with a radius $R = 300$ mm at our field gradient of $\mathrm{d}B/\mathrm{d}\rho = 2.8\,\mathrm{T/cm}$ for the group I elements in Table 1.

Table 1. The maximum guided velocity for the group-I elements ($\mu_{\text{eff}} = \mu_{\text{B}}$) in a quadrupole magnetic beam guide with $R = 300$ mm and $\mathrm{d}B/\mathrm{d}\rho = 2.8\,\mathrm{T/cm}$

Atom	^{1}H	^{6}Li	^{23}Na	^{39}K	^{85}Rb	^{133}Cs
v_m [m/s]	683	278	142	109	74	59

1 Quadrupole magnetic guides

1.1 Plane magnetic guide

The concept for plane magnetic multipole construction from hard permanent magnets has been expressed by Halbach [14]. For a segmented cylindrical quadrupole arrangement according to Fig. 1a the amplitude of the field strength depends on the transverse coordinate ρ through

$$B(\rho, z) = 2\rho B_{\text{R}} \left(\frac{1}{\rho_m} - \frac{1}{\rho_{\text{out}}} \right) G_2^N S_{\text{L}}(\rho, z) = 2.74\,\mathrm{T/cm} \times \rho\,[\mathrm{cm}] \times S_{\text{L}}(\rho, z)\,, \quad (2)$$

where B_{R} is the remanence force of the material (NdFeB: 1.1 T), and $\rho_m = 5$ mm and $\rho_{\text{out}} = 25$ mm (Fig. 1a) designate the inner and outer radii of the magnet assembly. The segmentation into eight homogeneously magnetized pie-shaped pieces is taken into account by a geometry factor $G_2^8 = 0.78$. The function $S_{\text{L}}(\rho, z)$ accounts for the fringe fields at the entrance and the exit of the beam guide and is unity for an infinitely long structure. The prediction of $\mathrm{d}B/\mathrm{d}\rho = 2.74\,\mathrm{T/cm}$ at the center of our quadrupoles according to (2) is well confirmed by the measured value of 2.8 T/cm. An experimentally favorable property of the axial magnet construction is the rapid decay of transverse external stray fields. At the longitudinal exits the field strength decreases with a scaling length on the order of the size of the aperture.

1.2 Curved magnetic beam guide potential: numerical treatment

The mechanical construction of the atomic beam guide is displayed in Fig. 1. Eight homogeneously magnetized segments are mounted into individual aluminum frames which have a wedge angle $2\alpha = 4.1°$. Six identical quadrupole wedges are then composed to make a 24.5° arc.

The analytical expression (2) is valid only for an idealized and plane, i.e., cylindrically straight quadrupole. For a more detailed treatment of our curved configuration we have therefore employed a numerical description of the magnetic field distribution which was subsequently used for numerical trajectory calculations.

It is known that the contribution of a homogeneously magnetized volume element (magnetization $\boldsymbol{M}$) to the magnetic potential Φ_{M} can be calculated from its equivalent surface charge contributions $\sigma_{\text{M}} = \boldsymbol{M} \cdot \boldsymbol{n}$, where $\boldsymbol{n}$ is the normal to the surface [15]. We have thus divided each magnet surface into small triangles (typical border length 0.1 mm, area S_Δ) with a concentrated point charge $Q_{\text{M}} = \sigma_{\text{M}} S_\Delta$ at the center of gravity of the triangle. The potential at a given point in space $\boldsymbol{r}$ is then approximately given by

$$\Phi_{\text{M}}(\boldsymbol{r}) = \int_{\text{Vol}} \mathrm{d}^3x' \frac{\nabla \cdot \boldsymbol{M}}{4\pi|\boldsymbol{r} - \boldsymbol{r}'|} = \int_{\text{Sur}} \mathrm{d}^2x' \frac{\sigma_{\text{M}}}{4\pi|\boldsymbol{r} - \boldsymbol{r}'|} \simeq \sum_i \frac{Q_{\text{M}}^i}{4\pi|\boldsymbol{r} - \boldsymbol{r_i}|}\,. \quad (3)$$

The discrete character of the charge distribution is important only in the immediate vicinity of the magnets on the scale of their typical separation. The potential in the volume of interest then is calculated on a grid with $\delta x = 0.2$ mm, $\delta y = 0.2$ mm, and $\delta z = 1.0$ mm. In the z direction we have chosen a wider grid since the variation of the potential in this direction is slow compared to that in the x, y directions. There is no advantage in further improving the accuracy since it is also limited at the same order of magnitude by variations of material properties (for example, direction and amplitude of the magnetization) as well as technical tolerances due to the construction.

For a test of the numerical model we have measured the magnetic field distribution of a single wedged quadrupole element by means of a commercial Hall probe. The active area of a few mm^2 causes spatial averaging and prevents accurate measurements of the field minimum near the axis. The agreement of measurement and numerical model is, however, satisfactory at the 1% level. In Fig. 2 the calculated field distribution is shown together with a result of the measurement.

To carry out trajectory simulations based on the numerical model potential a continuously varying magnetic field amplitude $\boldsymbol{B}(\boldsymbol{r}) = -\mu_0 \nabla \Phi_{\text{M}}(\boldsymbol{r})$ is made available through

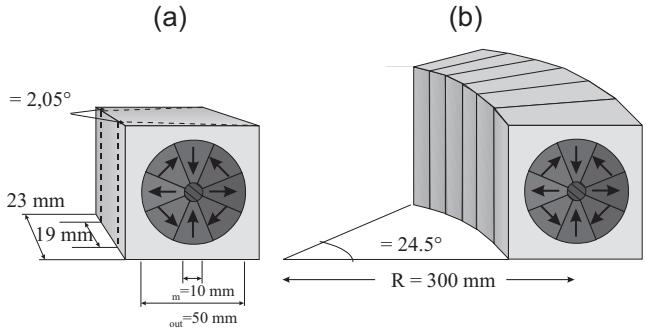

Fig. 1a,b. Construction of a curved magnetic quadrupole beam guide. **a** Each individual quadrupole is made from eight homogeneously magnetized pie-shaped segments (magnetization direction indicated by *arrows*). The wedge shape is indicated by the *dashed lines*. **b** Six wedged quadrupole elements are subsequently mounted together to form a 24.5° arc

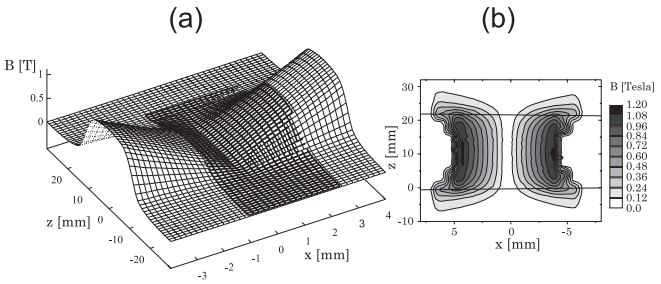

Fig. 2. a Measured magnetic field amplitude of one wedged quadrupole element (dark) in the $y = 0$ plane in comparison with the result of the numerical calculation. **b** Contour plot of the calculated magnetic field amplitude

a 4th-order polynomial interpolating the potential grid. The integration of the equation of motion then was performed by a 4th order Runge–Kutta method which was tested against the analytically known parabola solutions in an idealized ($S_L \equiv 1$) plane quadrupole potential of (2), yielding excellent agreement. In addition, energy conservation is tested to ensure the accuracy of the numerical calculations, especially near the axis of the toroid where the magnetic field vanishes and causes a singularity in the slope.

The simulations were carried out for an initial distribution of atoms at the beam guide entrance closely resembling the experimentally determined situation in both spatial and velocity coordinates. Several thousand trajectories were calculated for various initial velocities. For each velocity they were statistically analyzed with respect to transmission, vertical and horizontal beam profiles, and divergence on exit. Detailed results of this investigation are given along with experimental results.

1.3 Atomic motion in the beam guide

Atomic motion in a linear beam guide can be decomposed into longitudinal motion along its axis and into transverse motion, which are coupled only during entry or exit of a beam guide of finite length. In a circular toroid with bending radius R we can approximately use the same decomposition for estimates, where rotation along the torus can be taken into account by a suitable centrifugal potential. According to (1) the special case of circular orbits with radii between R and $R+\rho_m$ can only be obtained for atoms within a small range of velocities. For the sake of simplicity, however, we will define

$$v_m = \sqrt{R\frac{\beta}{m}} \tag{4}$$

as the maximum longitudinal velocity that can be deflected (cf. Table 1). Let us consider the transverse motion of an atom. Angular momentum with respect to the toroid axis is approximately conserved. Hence we can express the total energy E_{tot} approximately by ($\dot{x} = \mathrm{d}x/\mathrm{d}t$)

$$E_{\mathrm{tot}} \simeq \frac{m}{2}(\dot{x}^2+\dot{y}^2) + \beta\sqrt{x^2+y^2} + \frac{m v_0^2}{2}\left(1-\frac{2x}{R}\right) , \tag{5}$$

where v_0 is the longitudinal velocity, and the term in x/R accounts for an effective centrifugal potential due to rotation in the toroid.

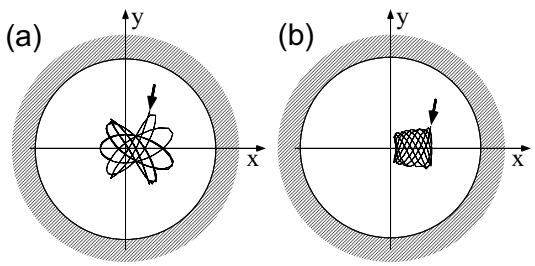

Fig. 3a,b. Examples of transverse trajectories in a toroidal quadrupole beam guide. Initial conditions at $t=0$ are indicated by arrow. **a** $(v_0/v_m)^2 = 0.3$, $\rho_i/\rho_m = 0.5$, $\phi_i = 1.0$ **b** $(v_0/v_m)^2 = 0.8$, $\rho_i/\rho_m = 0.5$, $\phi_i = 0.5$

It is natural to express the equations of motion in cylindrical coordinates (ρ, ϕ) with respect to the potential minimum axis of the torus. With $\beta R = m v_m^2$ and $\varepsilon = (v_0/v_m)^2$ and subtracting the rotational kinetic energy $\beta R\varepsilon/2$ along the torus we find instead of (5) the purely transverse condition

$$E_\perp = E_{\mathrm{tot}} - \beta R\varepsilon/2 = \frac{m}{2}\left(\dot{\rho}^2 + (\rho\dot{\phi})^2\right) + \beta\rho(1-\varepsilon\cos\phi) . \tag{6}$$

It is not integrable by elementary methods but can easily be used for numerical simulations to gain a better understanding of the trajectories in the beam guide. As an illustration we show two transverse trajectories in Fig. 3.

1.4 Stability conditions

In order to understand the general conditions for the confinement of atoms within the beam guide potential let us first estimate the influence of the fringe fields on atomic motion. Since we are working with collimated beams with a divergence of a few mrad only, a significant initial transverse velocity may only be imparted due to the fringe fields at the entrance of the beam guide where longitudinal and transverse motion are coupled. The fringe field in z direction extends over a length on the order of the bore cross section $2\rho_m$ of the beam guide. Therefore we can estimate the initial transverse velocity $v_\perp$ from an average fringe field acceleration $\beta/2m$ as

$$v_\perp \simeq \frac{\beta}{2m}\frac{2\rho_m}{v_0} , \tag{7}$$

which may safely be neglected for atomic velocities larger than 20 m/s as well as the associated change in the radial position. The initial transverse energy is hence well approximated by

$$E_\perp = \beta\rho_i\,(1-\varepsilon\cos\phi_i) , \tag{8}$$

depending on the radial coordinates on entrance into the beam guide only.

Atoms travelling at velocity v will be lost from the beam guide if they approach the outer circumference of the toroid at $(\rho_m, 0)$ with total transverse energy larger than the potential energy at that point,

$$E_\perp \geq E_{\mathrm{leak}} = \beta\rho_m(1-\varepsilon) . \tag{9}$$

For initial coordinates (ρ_i, ϕ_i) therefore an atom has to fulfill the condition

$$\beta\rho_i\,(1-\varepsilon\cos\phi_i) < \beta\rho_m(1-\varepsilon) , \tag{10}$$

which allows us to define a maximum initial radius acceptable for stable confinement of an atom inserted into the beam guide:

$$\rho_i = \rho_m\frac{1-\varepsilon}{1-\varepsilon\cos\phi_i} . \tag{11}$$

This condition is shown in Fig. 4 for comparison with the results of the numerical simulations. Atoms entering the beam

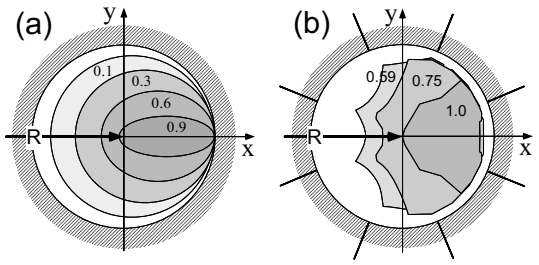

Fig. 4a,b. Insertion area of the beam guide cross section providing stable confinement for different parameters $\varepsilon = (v_0/v_m)^2$. If an atomic beam is restricted to this area, 100% transmission is achieved. **a** Analytical estimate for a 360° race track. **b** Numerical trajectory simulations for our 24.5° arc. The influence of the segmentation of the quadrupole (indicated by *black lines*) is clearly visible

guide with coordinates not fulfilling (11) may still be transmitted through a guide of finite length. For long guides, however, condition (11) gives a good limit since these atoms will eventually hit the magnets and get lost.

The transmission T of an infinitely long beam guide, if illuminated homogeneously across the aperture, is then given by the area enclosed by the ellipse of (11) normalized to the full cross section of the beam guide ($\pi\rho_m^2$):

$$T = \frac{\sqrt{1-\varepsilon^2}}{(1+\varepsilon)^2} \,. \tag{12}$$

This analytic approximation for the dependence of the transmission on ε and thus on the longitudinal velocity is shown in Fig. 5 along with numerical calculations and experimental results.

At very low initial velocities ($\varepsilon \ll 1$) the approximation is no longer valid, since longitudinal and transverse degrees of freedom get strongly coupled when an atom enters the fringe field. In addition, a significant fraction of atoms is reflected, although the beam guide potential minimum allows guidance of atoms at arbitrarily low energies. The onset of this effect is expected for longitudinal velocities on the order of the maximum allowed transverse velocity of about 10 m/s. This is confirmed by our numerical simulations.

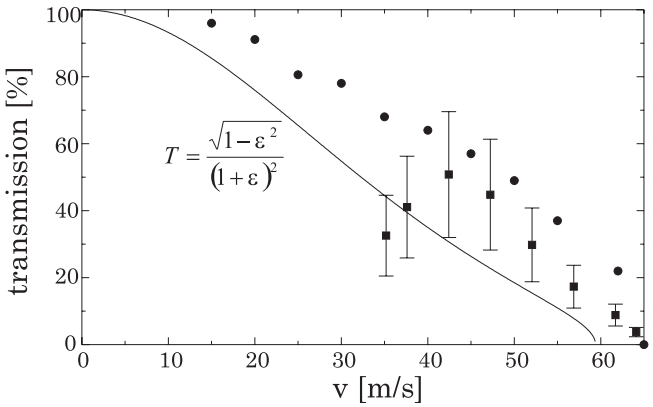

Fig. 5. Transmission of the 24.5° beam guide when illuminated homogeneously across the aperture. *Squares*: experimental results. *Circles*: numerical evaluation of trajectory calculations. The analytical estimate for infinitely long times is given by the *solid line*

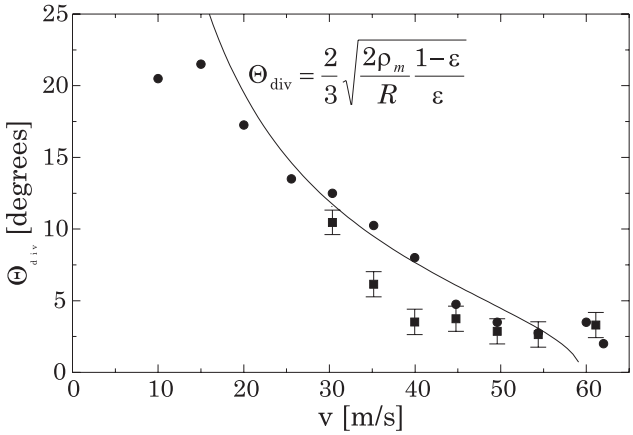

Fig. 6. Divergence angle of the atomic beam emerging from the beam guide. *Squares*: experimental results. *Circles*: numerical evaluation of trajectory calculations. *Solid line*: analytical estimate for infinitely long times

1.5 Divergence and acceptance angle

For efficient guiding it is necessary either to restrict the atomic beam extension to the elliptically shaped regions shown in Fig. 4, or to focus an atomic beam onto the entrance of the beam guide, in close analogy to optical waveguides. It is therefore important to understand the tolerable divergence as a function of velocity. For an analytical estimate let us consider the inverse problem and calculate the angular spread of guided atoms when they leave the toroid. For this purpose we assume that dynamic evolution of atomic trajectories has already homogeneously populated phase space at the energy shell corresponding to the initial transverse energy $E_\perp$ of (8) at the output. Integration across the insertion ellipse of (11) yields

$$\langle E_\perp^{\rm ini}\rangle = \beta\rho_m \frac{2}{3}(1-\varepsilon) \,. \tag{13}$$

A measure for the average transverse velocity spread $v_{\rm div}^2 = \langle v_x^2 + v_y^2\rangle$ may be obtained from the equipartition theorem which in this case reads $\langle m(v_x^2+v_y^2)/2\rangle = 2/3\langle E_\perp^{\rm ini}\rangle$. The divergence angle $\Theta_{\rm div}$ is then evaluated from $m v_{\rm div}^2 = \beta R\varepsilon(v_{\rm div}/v_0)^2$:

$$\Theta_{\rm div} \simeq \frac{v_{\rm div}}{v_0} = \frac{2}{3}\sqrt{\frac{2\rho_m}{R}\frac{1-\varepsilon}{\varepsilon}} \,. \tag{14}$$

This simple estimate is in good agreement with experimental results and numerical simulations, as shown in Fig. 6.

2 Experimental setup

The general experimental setup is schematically shown in Fig. 7. For our experiments we used a cesium atomic beam which was slowed by the Zeeman technique [16]. All laser light was derived from grating-tuned diode lasers [17] stabilized onto cesium vapor cells by Doppler-free spectroscopy techniques. The Zeeman slower is 1.4 m long and sustains a Doppler compensation field which decreases in a parabolic shape towards the end of the slower and can be tuned to an

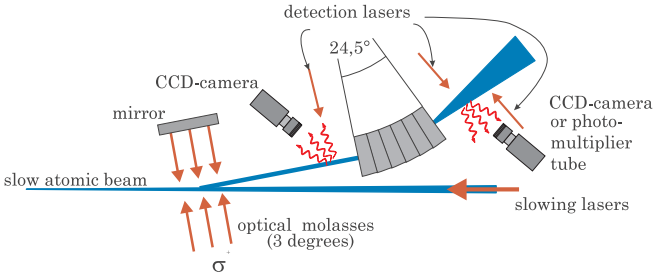

Fig. 7. Atomic beam apparatus: a Zeeman-slowed cesium atomic beam first is slightly deflected by an optical molasses section and afterwards inserted into a 24.5° arc of a quadrupole magnetic beam guide

initial maximum value of 22 mT. Furthermore, a homogeneous bias field of $B_{\text{bias}} = 22$ mT is applied in order to suppress depopulation pumping due to imperfect laser polarization. The final velocity is selected by adjusting the frequency of the slowing laser. The laser is σ^+ polarized, so the atoms leave the Zeeman slower in the $(F = 4, m_F = 4)$ state. For the experiments described here we have determined a longitudinal velocity width (FWHM) varying from 15 m/s to 30 m/s for average velocities from 100 m/s to 25 m/s by Doppler-sensitive measurement of the atomic beam fluorescence spectrum excited by a laser crossing the atomic beam at an angle of 23°. The velocity distribution is substantially larger than the expected Doppler width of order 1 m/s but sufficiently narrow for the experiments described here. We attribute this deviation to the cutoff condition which was not steep enough to cause a sufficiently rapid cutoff of the slowing process. An improved experimental setup has in the meantime resulted in a velocity width approaching the theoretically expected value. Details of this Zeeman slower for cesium atoms will be published elsewhere.

Before atoms were inserted into the beam guide a slightly tilted transverse optical molasses section was used to deflect the slow atomic beam by 3° from the axis. A Gaussian-shaped laser beam with a cross section of 3×1 cm and a total laser power of 13 mW is circularly polarized and back-reflected by a mirror. A small magnetic field applied parallel to the laser beam ensures that the atoms leave the molasses light field predominantly in the low-field seeking magnetic state $(F = 4, m_F = 4)$ required for proper magnetic guiding. The residual transverse velocity spread is about 0.5 m/s. After 400 mm of free flight the beam guide could be mounted onto the axis of the deflected atomic beam without obstructing the path for the cooling laser light. The atomic beam at this point had a Gaussian beam profile with a diameter of 2.5 cm and fully covered the aperture of the magnetic beam guide.

3 Experimental results

Important properties of a beam guidance device are the transmission and the acceptance or divergence angle. The transmission was determined by monitoring the resonance fluorescence at the exit with a photo multiplier tube and comparing it to the fluorescence signal of atoms entering the beam guide, which was measured with a CCD camera. Beam profiles and divergence angle of the transmitted atomic beam were measured from spatially resolved CCD pictures of the fluorescence distribution.

3.1 Transmission measurement

For a measurement of the incident flux the atomic beam was illuminated by a Gaussian laser beam of width $2w = 1$ cm and located approximately 2 cm in front of the entrance to the magnetic guide. The influence of the magnetic fringe field on the fluorescence distribution is taken into account by an average detuning between laser and atom which grows linearly with radial separation from the magnetic guide axis (the quadrupole field maintains a linear growth of the magnetic field amplitude in the fringe field, too). Taking into account the spatial distribution of the laser light field and the saturation of atomic transitions, good agreement of the CCD camera fluorescence profiles with the expected spatial distribution from a Gaussian-shaped atomic beam is found. In the end, the flux of atoms entering the beam guide aperture is determined from the fluorescence intensity except for a calibration factor that only depends on the overall efficiency of the CCD camera. It decreases with decreasing velocity since the flux of slow atoms extracted from the Zeeman slower is reduced, the beam divergence increases, and because beam attenuation due to collisions with the background gas becomes increasingly important. Note that the estimated loss rate at a base pressure of $p = 10^{-5}$ Pa is $R_{\text{loss}} \simeq 60\,\text{s}^{-1}$, corresponding to a mean free path of less than 1 m for atoms with $v = 50$ m/s. We would like to mention that this pressure is not limited by the permanent magnets. The outgassing rate of the material is comparable with unbaked aluminum or stainless steel, they are bakeable up to 100 °C, and we have achieved a base pressure in the 10^{-7} Pa range in a different setup.

On the exit side we have determined the flux at a distance of 5 cm from the magnetic guide where fringe fields are negligible. In this case a photomultiplier tube was used to record the fluorescence intensity by scanning a probe laser across the atomic resonance. Taking into account the measured laser beam properties and the vertical atomic beam profiles obtained from the numerical simulations the variation of the relative transmitted flux with atomic beam velocity is determined. An absolute calibration of the transmission was performed by simultaneously recording the fluorescence of atoms at the exit with the photomultiplier tube and the CCD camera for one velocity class.

The experimental results (Fig. 5) are in reasonable agreement with our simulation for velocities between 40 and 65 m/s. It is not surprising that both the simulation and the experiment show larger transmission than expected according to (12) which was derived for arbitrarily long guidance times. Below 40 m/s a rapid reduction of the transmission is observed which is not yet fully understood.

Whether an atom is transmitted or not crucially depends on the initial position at the entrance. Therefore, 100 % transmission can be achieved if the incident beam enters within the insertion regions shown in Fig. 4 as a function of velocity. This may be accomplished, for instance, by slightly focusing the atomic beam onto the entrance with a magnetic lens [18].

3.2 Beam profiles

We have determined beam profiles of the emanating atomic beam at a distance of 3.5 cm from the guide. In order to suppress the influence of the magnetic fringe fields on the measurement the detection laser beam frequency was periodically

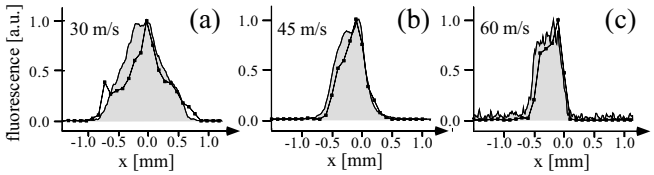

Fig. 8a–c. Normalized atomic beam fluorescence profiles in the horizontal plane 3.5 cm behind the exit of the beam guide as measured with the CCD camera. Negative (positive) x-values correspond to a deflection of less (more) than 24.5°. **a–c**: Profiles for velocities $v = 30,\ 45,\ 60$ m/s. *Shaded areas*: experimental results. *Squares*: results of trajectory simulations

swept across the spectral line during illumination. For various velocities CCD images of the horizontal (i.e., in the plane of deflection) distribution of the fluorescence intensity were recorded and analyzed. Results are given in Fig. 8 and show good agreement with the numerical trajectory calculations.

3.3 Divergence measurement

The divergence of the deflected atomic beam was determined by recording the atomic beam fluorescence in the plane of deflection with a CCD camera at two distances of 3.5 and 5 cm, respectively, from the exit of the magnetic guide. The laser frequency was again periodically modulated across the spectral distribution of atomic resonance frequencies. One finds a good agreement of simulation, experimental data, and the crude estimate of (14) as shown in Fig. 6.

The measured divergence on one hand indicates a large acceptance angle at the entrance of the beam guide which provides efficient loading. On the other hand, it leads to a rapid reduction of atomic flux density behind the exit. This can be overcome by applying a two-dimensional magneto-optical compression section within the fringe field of the magnetic beam guide.

4 Conclusion

We have demonstrated that a magnetic guide made from strong permanent magnets can efficiently deflect even heavy atoms over large angles and at moderate velocities, in our case from 30 m/s to 60 m/s, the maximum tolerable velocity. The overall good agreement of trajectory simulations and experimental results lends confidence to the engineering of permanent magnetic guidance systems for atomic beams.

Assuming a small longitudinal magnetic field of 10^{-4} T to prevent on-axis spin-flips the mode spacing of the lowest vibrational modes is estimated to be $2\pi \times 30$ kHz corresponding to a temperature of 1.3 μK. Thus it seems feasible to achieve effectively one-dimensional atomic systems in similar geometries.

Acknowledgements. We wish to thank I. Bloch and M. Kreis for help in the experiment. The Deutsche Forschungsgemeinschaft has financially supported this work under contract Me 971/3.

References

1. C.S. Adams, M. Sigel, J. Mlynek: Phys. Rep. **240**, 143 (1994)
2. W. Ketterle, D.E. Pritchard: Appl. Phys. B **54**, 403 (1992)
3. J. Richmond, S.N. Chormaic, B. Cantwell, G. Opat: Act. Phys. Slov. **48**, 481 (1998)
4. E.A. Hinds, M.G. Boshier, I.G. Hughes: Phys. Rev. Lett. **80**, 645 (1998)
5. J. Schmiedmayer: Appl. Phys. B **60**, 169 (1995)
6. M. A. Ol'Shanii, Y.B. Ovchinnikov, V.S. Lethokov: Opt. Commun. **98**, 77 (1993)
7. M.J. Renn, D. Montgomery, O. Vdovin, D.Z. Anderson, C. E. Wieman, E.A. Cornell: Phys. Rev. Lett. **75**, 3253 (1995)
8. M.J. Renn, E.A. Donley, E.A. Cornell, C.E. Wieman, D.Z. Anderson: Phys. Rev. A **53**, R648 (1996)
9. H. Ito, K. Sakaki, M. Ohtsu, W. Jhe: Appl. Phys. Lett. **70**, 2496 (1997)
10. C.J. Myatt, E.A. Burt, R.W. Ghrist, E.A. Cornell, C.E. Wieman: Phys. Rev. Lett. **78**, 586 (1997)
11. S. Kuppens, M. Rauner, M. Schiffer, K. Sengstock, W. Ertmer: Phys. Rev. A **58**, 3068 (1998)
12. H. Monien, M. Linn, N. Elstner: Phys. Rev. A **58**, R3395 (1998)
13. K.J. Kügler, W. Paul, J. Trinks: Nucl. Instrum. Methods A **228**, 240 (1985); W. Paul, F. Anton, L. Paul, S. Paul, W. Mampe: Z. Phys. C **45**, 25 (1989); W. Paul: *Laser Manipulation of Atoms and Ions*, ed. by E. Arimondo, W.D. Phillips, F. Strumia (North-Holland, Amsterdam 1992)
14. K. Halbach: Nucl. Instrum. Methods **169**, 1 (1980)
15. J.D. Jackson: *Classical Electrodynamics* (John Wiley, New York 1975)
16. W.D. Phillips, H. Metcalf: Phys. Rev. Lett. **48**, 596 (1982)
17. L. Ricchi, M. Weidemüller, T. Esslinger, A. Hemmerich, C. Zimmermann, V. Vuletic, W. König, T.W. Hänsch: Opt. Commun. **117**, 541 (1995)
18. W.G. Kaenders, F. Lison, I. Müller, A. Richter, R. Wynands, D. Meschede: Phys. Rev. A **54**, 5067 (1996)